

Audiovisual Probabilistic Tracking of Multiple Speakers in Meetings

Daniel Gatica-Perez, *Member, IEEE*, Guillaume Lathoud, Jean-Marc Odobez, *Member, IEEE*, and Iain McCowan, *Member, IEEE*

Abstract—Tracking speakers in multiparty conversations constitutes a fundamental task for automatic meeting analysis. In this paper, we present a novel probabilistic approach to jointly track the location and speaking activity of multiple speakers in a multisensor meeting room, equipped with a small microphone array and multiple uncalibrated cameras. Our framework is based on a mixed-state dynamic graphical model defined on a multiperson state-space, which includes the explicit definition of a proximity-based interaction model. The model integrates audiovisual (AV) data through a novel observation model. Audio observations are derived from a source localization algorithm. Visual observations are based on models of the shape and spatial structure of human heads. Approximate inference in our model, needed given its complexity, is performed with a Markov Chain Monte Carlo particle filter (MCMC-PF), which results in high sampling efficiency. We present results—based on an objective evaluation procedure—that show that our framework 1) is capable of locating and tracking the position and speaking activity of multiple meeting participants engaged in real conversations with good accuracy, 2) can deal with cases of visual clutter and occlusion, and 3) significantly outperforms a traditional sampling-based approach.

Index Terms—Meetings, Monte Carlo methods, multimodal fusion, tracking.

I. INTRODUCTION

THE automatic analysis of meetings recorded in multisensor rooms is an emerging research field in various domains, including audio and speech processing, computer vision, human-computer interaction, and information retrieval [8], [10], [24], [31], [33], [42], [47], [49]. Analyzing meetings poses a diversity of technical challenges, and opens doors to a number of relevant applications, including automatic structuring and indexing of meeting collections, and facilitation of remote meetings.

In the context of meetings, localizing and tracking people and their speaking activity play fundamental roles in two areas. The

first one is media processing: speaker location is useful to select or steer a camera as part of a visualization or production model, to enhance the audio stream via microphone-array beamforming for speech recognition, to provide accumulated information for person identification, and to recognize location-based events (e.g., a presentation). The second one is human interaction analysis: social psychology has highlighted the role of nonverbal behavior (e.g., gaze and facial expressions) in interactions, and the correlation between speaker turn patterns and aspects of the behavior of a group [32]. Extracting cues to identify such multimodal behaviors requires reliable speaker tracking.

Although the tracking task in meetings is facilitated by the constraints of the physical space and the expected type of human activities, the multimodal multispeaker tracking problem poses various challenges. These include algorithms for audiovisual (AV) data fusion, that make use of the modalities' complementarity, and for tractable joint multiperson models (which represent each individual state, while accounting for the constraints introduced by their interaction). In meetings, interaction in its simplest form relates to proximity in the visual modality (occlusion being the fundamental case), and to overlapping speech in the audio modality (commonly found in spontaneous conversations [39]). Approaches addressing some of these issues have begun to appear [5], [6].

In this paper, we address the problem as one of approximate inference in a dynamical graphical model, using particle filtering (PF) techniques [11], [18], building on recent advances in the field [22]. For a state-space model, a PF recursively approximates the filtering distribution of states given observations, using a dynamical model, an observation model, and sampling techniques, by predicting candidate configurations and measuring their likelihood. Our model uses a mixed-state, multiobject state-space, which in addition to being mathematically rigorous, allows for the integration of a pairwise person occlusion model through the addition of a Markov random field (MRF) prior in the multiobject dynamic model. To address the problems of traditional PFs in handling high-dimensional spaces (defined by the joint multiobject configurations), we combine Markov Chain Monte Carlo (MCMC) techniques with the PF framework, allowing for efficient sampling [22], [29]. Our work integrates data captured by a small microphone array and multiple cameras with mostly nonoverlapping fields-of-view through the definition of a novel observation model of AV features. Based on an objective evaluation of the quality of estimated head location and speaking activity, and using small-group discussion data, we show that our framework is capable of jointly tracking the location and speaking activity

Manuscript received July 7, 2005; revised March 30, 2006. This work was supported by the Swiss National Center of Competence in Research on Interactive Multimodal Information Management (IM2), and the EC projects Augmented Multiparty Interaction (AMI, publication AMI-151), and Hearing Organization and Recognition of Speech in Europe (HOARSE), all through the Swiss Federal Office for Education and Science (OFES). The associate editor coordinating the review of this manuscript and approving it for publication was Dr. Michael Davies.

D. Gatica-Perez, G. Lathoud, and J.-M. Odobez are with the IDIAP Research Institute and Ecole Polytechnique Federale de Lausanne (EPFL), CH-1920 Martigny, Switzerland (e-mail: gatica@idiap.ch; lathoud@idiap.ch; odobez@idiap.ch).

I. McCowan is with the eHealth Research Centre, Brisbane, Queensland 4000, Australia (e-mail: iain.mccowan@csiro.au).

Digital Object Identifier 10.1109/TASL.2006.881678

of multiple meeting participants with good accuracy, dealing with realistic conditions, and outperforming a traditional PF model.

The paper is organized as follows. Section II discusses related work. After summarizing our framework in Section III, Sections IV–VII present, in order, the multiperson dynamical model, the multiperson AV observation model, the inference technique, and the algorithm for handling varying numbers of people. Section VIII describes and discusses experiments and results. Finally, Section IX provides some conclusions.

II. RELATED WORK

Localizing and tracking speakers in enclosed spaces using AV information has increasingly attracted attention in signal processing and computer vision [1], [3], [5]–[7], [13], [14], [17], [35], [37], [44], [50], given the complementary characteristics of each modality. Broadly speaking, the differences among existing works arise from the overall goal (tracking single versus multiple speakers), the specific detection/tracking framework, and the AV sensor configuration. Much work has concentrated on the single-speaker case, assuming either single-person scenes [1], [7], [35], or multiperson scenes where only the location of the current speaker is tracked [3], [13], [14], [17], [37], [44], [50]. Many of these works use simple sensor configurations (e.g., one camera and a microphone pair) [3], [7], [35], [44]. Among the existing techniques, probabilistic generative models based on exact [35] or approximate inference methods (both variational [3] and sampling-based [44], [50]) appear to be the most promising, given their principled formulation and demonstrated performance.

None of the above works can handle the problem addressed here: continuously inferring, from audio and video data, the location and speaking status for several people in a realistic conversational setting. In fact, although audio-based multispeaker tracking and vision-based multiperson tracking have been studied for a few years as separate problems in signal processing [26], [38], [43], [46], [48] and computer vision [20], [36], respectively, the AV multispeaker tracking problem has been studied relatively recently, making use of more complex sensor configurations [5], [6], [8], [21], [40]. While single cameras are useful for remote conferencing applications, multiperson conversational settings like meetings often call for the use of multiple cameras and microphones to cover an entire workspace (table, whiteboards, etc.) [5], [6], [8]. More specifically, Cutler *et al.* [8] described a system based on a device that integrates a small circular microphone array and several calibrated cameras, whose views are composed into a panorama. The tracking system, in which each person is tracked independently, consists of three modules: AV auto-initialization, (using either a standard acoustic source localization algorithm or visual cues), visual tracking using a hidden Markov model (HMM), and tracking verification. Kapralos *et al.* [21] described a nonprobabilistic multispeaker detection algorithm using an omnidirectional camera (which has limitations of resolution) and a microphone array, calibrated with respect to each other. At each video frame, the method extracts skin-color blobs by traditional techniques, and then detects a sound source using standard beamforming on the small set of directions indicated

by the skin-blob locations. Siracusa *et al.* [40] described an AV multispeaker tracking system, based on a stereo camera and a linear microphone array, consisting of three separate modules: stereo-based visual tracking of three-dimensional (3-D) head location and pose for each person independently, estimation of the audio signal’s direction of arrival with the microphone array, and estimation of audiovisual synchronous activity. Two hypothesis tests are used to make independent decisions about the speaking activity and visual focus of the speakers, based on simple statistical models defined on the observations derived from each module.

To the best of our knowledge, the closest works to ours are [5], [6], both based on PF techniques. Checka *et al.* [5] used two calibrated cameras and four linear submicrophone arrays on a wall, and was based on the model proposed by Isard and MacCormick [20], defining a multiperson state-space in which the number of people can vary over time. A full-body multiperson observation model was defined by two terms: one for video, derived from a pixelwise background subtraction model, and one for audio, derived from a set of short-time Fourier transforms computed on each microphone’s signal. The PF relied on importance sampling, and is thus likely to become inefficient as the number of objects increases. Chen and Rui [6] used the same calibrated sensor setup as Cutler *et al.* [8], and tracked multiple speakers with a set of independent PFs, one for each person. Each PF uses a mixture proposal distribution, in which the mixture components are derived from the output of single-cue trackers (based on audio, color, and shape information). This proposal increases robustness in case of tracking failures in single modalities.

As we describe in the remainder of the paper, our work substantially differs from previous work in AV multispeaker tracking with respect to the choices for the multiperson dynamical model, the AV observation model, and the sampling mechanism. Building on the model recently proposed by Khan *et al.* [22], our model has two advantages over the works of Checka *et al.* [5] and Chen and Rui [6]. First, unlike both [5] and [6], we use a multiperson dynamical model that explicitly incorporates a pairwise person interaction prior term. This model is especially useful to handle person occlusion. Second, unlike [5] and [6], we use efficient MCMC sampling techniques that allow to jointly track several objects in a tractable manner (effectively close to the case of independent PFs), while preserving the rigorous joint state-space formulation. Finally, we objectively evaluate the performance of our algorithm, in more detail than that of [5], [6].

III. MODEL FORMULATION

We use a generative approach to model the tracking problem [11], [18]. Given a Markov state-space model, with hidden states \mathbf{X}_t representing the joint multiobject configuration (e.g., position, scale, etc.), and AV observations \mathbf{Y}_t , the filtering distribution $p(\mathbf{X}_t|\mathbf{Y}_{1:t})$ of \mathbf{X}_t given the observations $\mathbf{Y}_{1:t} = (\mathbf{Y}_1, \dots, \mathbf{Y}_t)$ up to time-step t can be recursively computed using Bayes’ rule by

$$p(\mathbf{X}_t|\mathbf{Y}_{1:t}) \propto p(\mathbf{Y}_t|\mathbf{X}_t) \int_{\mathbf{X}_{t-1}} p(\mathbf{X}_t|\mathbf{X}_{t-1})p(\mathbf{X}_{t-1}|\mathbf{Y}_{1:t-1})d\mathbf{X}_{t-1} \quad (1)$$

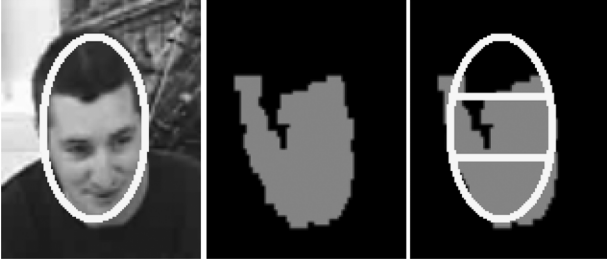


Fig. 1. Spatial structure observations. Given a configuration (in white), and a skin blob (in gray), part-based precision/recall features are computed from the spatial support of configuration parts and blob.

where $p(\mathbf{X}_t|\mathbf{X}_{t-1})$ is the multiobject dynamical model of the temporal evolution of the multiobject state-space, and $p(\mathbf{Y}_t|\mathbf{X}_t)$ denotes the multiobject observation likelihood, which measures how well the observations fit the multiobject predictions.

PFs approximate (1) for nonlinear, non-Gaussian problems [11]. From the various available formulations, we follow the one described by Isard and Blake [18]. The basic PF represents the filtering distribution using a weighted set of N samples $\{(\mathbf{X}_t^{(n)}, w_t^{(n)}), n = 1, \dots, N\}$, where $\mathbf{X}_t^{(n)}$ and $w_t^{(n)}$ denote the n th sample and its associated weight at each time-step, and updates this representation as new data arrive. With this representation, (1) can be approximated by a mixture model

$$p(\mathbf{X}_t|\mathbf{Y}_{1:t}) \approx \mathcal{Z}^{-1} p(\mathbf{Y}_t|\mathbf{X}_t) \sum_n w_{t-1}^{(n)} p(\mathbf{X}_t|\mathbf{X}_{t-1}^{(n)}) \quad (2)$$

using importance sampling (\mathcal{Z} is a normalization constant). Given the particle set at the previous time-step, $\{(\mathbf{X}_{t-1}^{(n)}, w_{t-1}^{(n)})\}$, a set of new configurations at the current time-step are drawn from a proposal distribution $q(\mathbf{X}_t) = \sum_r w_{t-1}^{(r)} p(\mathbf{X}_t|\mathbf{X}_{t-1}^{(r)})$. The weights are then computed as $w_t^{(n)} \propto p(\mathbf{Y}_t|\mathbf{X}_t^{(n)})$.

A state at time-step t is defined by $\mathbf{X}_t = (\mathbf{X}_{i,t}), i \in \mathcal{I}_t$, where \mathcal{I}_t is the set of object identifiers in the configuration, $m_t = |\mathcal{I}_t|$ denotes the number of objects, and $|\cdot|$ indicates set cardinality. Each object has a unique identifier, given by the position occupied by their configuration in the state vector. In what follows, we assume \mathcal{I}_t to be fixed (the case when \mathcal{I}_t varies over time is discussed in Section VII). A mixed state-space is defined for single-object configurations $\mathbf{X}_{i,t}$, where both the geometric transformations of a person's model in the image plane and the speaking activity are tracked. In the specific implementation described in this work, a person is represented by the elliptical silhouette of the head in the image plane (Fig. 1, left). Furthermore, a single-object state $\mathbf{X}_{i,t} = (\mathbf{x}_{i,t}, k_{i,t})$ is composed of a 3-D continuous vector $\mathbf{x}_{i,t} = (u_{i,t}, v_{i,t}, s_{i,t})$, defined over a subspace of affine transformations comprising two-dimensional (2-D) translation and scaling, and a discrete binary variable $k_{i,t}$, which models each participant's speaking status (0: silent, 1: speaking).

The generative model in (1) and its approximation in (2) require the specification of the dynamical and observation models. Additionally, the dimension of the multiobject state-space grows linearly with the number of objects, so that even for a small-group discussion (4–5 participants) and the

compact single-object state-space described above, the dimension of the joint state-space is prohibitively high for importance sampling techniques, which calls for a more efficient sampling scheme. These issues are discussed in the following sections.

IV. MULTIOBJECT DYNAMICAL MODEL

The dynamical model includes two factors: one that describes interaction-free, single-object dynamics, and another one that explicitly models interactions (e.g., occlusion), constraining the dynamics of each object based on the state of the others, via a pairwise MRF prior [22], [27]. The field is defined on an undirected graph, where the graph vertices are the objects, and the links are defined between object pairs at each time-step. The dynamical model is expressed as

$$p(\mathbf{X}_t|\mathbf{X}_{t-1}) \propto \left(\prod_{i \in \mathcal{I}_t} p(\mathbf{X}_{i,t}|\mathbf{X}_{i,t-1}) \right) \left(\prod_{(i,j) \in \mathcal{C}} \phi(\mathbf{X}_{i,t}, \mathbf{X}_{j,t}) \right) \quad (3)$$

where $p(\mathbf{X}_{i,t}|\mathbf{X}_{i,t-1})$ denotes the dynamics of the i th object, and the prior is a product of pairwise potentials, denoted by $\phi(\mathbf{X}_{i,t}, \mathbf{X}_{j,t})$ over the set of cliques \mathcal{C} (i.e., pairs of connected nodes) in the graph. The approximation in (2) is now given by

$$p(\mathbf{X}_t|\mathbf{Y}_{1:t}) \approx \mathcal{Z}^{-1} p(\mathbf{Y}_t|\mathbf{X}_t) \left(\prod_{(i,j) \in \mathcal{C}} \phi(\mathbf{X}_{i,t}, \mathbf{X}_{j,t}) \right) \times \left(\sum_n w_{t-1}^{(n)} \prod_{i \in \mathcal{I}_t} p(\mathbf{X}_{i,t}|\mathbf{X}_{i,t-1}^{(n)}) \right) \quad (4)$$

where the interaction term can be moved out of the sum over particles, as it does not depend on past information. Furthermore, assuming that the motion and the speaking activity are independent, each single-object dynamical model is factorized as

$$p(\mathbf{X}_{i,t}|\mathbf{X}_{i,t-1}) = p(\mathbf{x}_{i,t}|\mathbf{x}_{i,t-1}) p(k_{i,t}|k_{i,t-1}) \quad (5)$$

where the continuous distribution $p(\mathbf{x}_{i,t}|\mathbf{x}_{i,t-1})$ is modeled as a second-order auto-regressive model [18], and

$$p(k_{i,t}|k_{i,t-1}) = \begin{bmatrix} \beta_{00} & \beta_{01} \\ \beta_{10} & \beta_{11} \end{bmatrix}$$

is a 2×2 transition probability matrix (TPM) with parameters $\{\beta_{00}, \beta_{01}, \beta_{10}, \beta_{11}\}$, with $\beta_{01} = 1 - \beta_{00}$ and $\beta_{10} = 1 - \beta_{11}$.

The interaction model we adopt takes into account visual information, and penalizes large visual overlaps between objects [22], which reduces the possibility of associating two configurations to one single object when people occlude each other momentarily. Let $\mathcal{S}_{i,t}$ and $\mathcal{S}_{j,t}$ denote, respectively, the 2-D sets corresponding to the spatial supports of $\mathbf{x}_{i,t}$ and $\mathbf{x}_{j,t}$, i.e., the application of the continuous transformation to the object templates on the image plane. The spatial overlap measures used in this paper are the well-known precision (ν) and recall (ρ) measures from information retrieval [2]. Assuming that $\mathcal{S}_{i,t}$ is the reference, the measures are defined by

$$\nu(\mathcal{S}_{i,t}, \mathcal{S}_{j,t}) = \frac{|\mathcal{S}_{i,t} \cap \mathcal{S}_{j,t}|}{|\mathcal{S}_{j,t}|}, \quad \rho(\mathcal{S}_{i,t}, \mathcal{S}_{j,t}) = \frac{|\mathcal{S}_{i,t} \cap \mathcal{S}_{j,t}|}{|\mathcal{S}_{i,t}|} \quad (6)$$

Such measures are effective to quantify spatial overlap. Both precision and recall take their maximum value (unity) when the spatial support of two objects perfectly match, and their minimum (zero) when the objects have no overlap. In this paper, by using the fact that $\nu(\mathcal{S}_{i,t}, \mathcal{S}_{j,t}) = \rho(\mathcal{S}_{j,t}, \mathcal{S}_{i,t})$, we define the (symmetric) pairwise potentials in the MRF to be

$$\phi(\mathbf{X}_{i,t}, \mathbf{X}_{j,t}) \propto \exp(-\lambda_\phi (\nu(\mathcal{S}_{i,t}, \mathcal{S}_{j,t}) + \rho(\mathcal{S}_{i,t}, \mathcal{S}_{j,t}))) \quad (7)$$

where λ_ϕ is a model parameter. With this definition, a perfect match between the spatial support of two objects corresponds to the minimum value of $\phi(\cdot, \cdot)$, effectively penalizing such object overlap. In contrast, a null overlap between two objects corresponds to the maximum value of $\phi(\cdot, \cdot) \propto 1$.

V. AUDIOVISUAL OBSERVATION MODEL

Observation models are derived from audio and video. Both shape and spatial structure of human heads are used as visual cues, so the three types of observations are defined as $\mathbf{Y}_t = (\mathbf{Y}_t^a, \mathbf{Y}_t^{sh}, \mathbf{Y}_t^{st})$, where the superindices stand for *audio*, *shape*, and *spatial structure*, respectively. As other works (e.g., [36]), we further assume that observations are extracted for each object, and that the different observations are conditionally independent given the single-object states, producing the following factorized representation:

$$\begin{aligned} p(\mathbf{Y}_t | \mathbf{X}_t) &= \prod_{i \in \mathcal{I}_t} p(\mathbf{Y}_{i,t} | \mathbf{X}_{i,t}) \\ &= \prod_{i \in \mathcal{I}_t} p(\mathbf{Y}_{i,t}^a | \mathbf{X}_{i,t}) p(\mathbf{Y}_{i,t}^{sh} | \mathbf{X}_{i,t}) p(\mathbf{Y}_{i,t}^{st} | \mathbf{X}_{i,t}). \end{aligned} \quad (8)$$

All terms in (8) are defined in the following subsections.

A. Audio Observations

Audio observations are derived from the microphone array signals to produce 2-D location estimates in the corresponding image plane. The audio observation likelihood is then defined using such estimates. The procedure consists of three steps: audio source localization, speech/nonspeech classification, and mapping of speaker location estimates onto the image plane [14]. Each of these steps are described in the following subsections.

1) *Source Localization*: A simple single source localization technique based on time delay of arrival (TDOA) is used to generate candidate 3-D speaker locations. In particular, we use the steered response power–phase transform (SRP-PHAT) measure [9], due to its low computational requirements and suitability for reverberant environments.

We define a vector of theoretical time-delays associated with a 3-D location $Z \in \mathbb{R}^3$ as $\boldsymbol{\tau}^Z \triangleq (\tau^{1,Z}, \dots, \tau^{\psi,Z}, \dots, \tau^{N_\psi,Z})$, where N_ψ is the number of pairs and $\tau^{\psi,Z}$ is the delay (in samples) between the microphones in pair ψ , defined as $\tau^{\psi,Z} = (f_s/c_s)(\|Z - M_1^\psi\| - \|Z - M_2^\psi\|)$, where $M_1^\psi, M_2^\psi \in \mathbb{R}^3$ are the locations of the microphones in pair ψ , $\|\cdot\|$ is the Euclidean norm, f_s the sampling frequency, and c_s the speed of sound. Note that for a given time-delay τ_0 and pair ψ , there exists a hyperboloid of locations Z satisfying $\tau^{\psi,Z} = \tau_0$.

From two signals $\mathbf{s}_1^\psi(t)$ and $\mathbf{s}_2^\psi(t)$ of a given microphone pair ψ , the frequency-domain GCC-PHAT [23], denoted by $G_{\text{PHAT}}^\psi(f)$, is defined as

$$G_{\text{PHAT}}^\psi(f) \triangleq \frac{\mathbf{S}_1^\psi(f) \cdot [\mathbf{S}_2^\psi(f)]^*}{|\mathbf{S}_1^\psi(f) \cdot [\mathbf{S}_2^\psi(f)]^*|} \quad (9)$$

where $\mathbf{S}_1^\psi(f)$ and $\mathbf{S}_2^\psi(f)$ are Fourier transforms of the two signals and $[\cdot]^*$ denotes the complex conjugate. Typically the two Fourier transforms are estimated on Hamming-windowed segments of 20–30 ms. By performing an inverse Fourier transform, and summing the time-domain GCC-PHAT $R_{\text{PHAT}}^\psi(\tau)$ across pairs, we obtain the SRP-PHAT measure

$$P_{\text{SRP-PHAT}}(Z) \triangleq \sum_{\psi=1}^{N_\psi} R_{\text{PHAT}}^\psi(\tau^{\psi,Z}). \quad (10)$$

From this, the source location is estimated as

$$\hat{Z} = \arg \max_{Z \in \mathbb{R}^3} [P_{\text{SRP-PHAT}}(Z)]. \quad (11)$$

From geometrical considerations, at least three microphone pairs ($N_\psi \geq 3$) are required to obtain a unique peak.

The maximization is implemented through exhaustive search over a fixed grid of points, $H \subset \mathbb{R}^3$ such that $\forall Z \in \mathbb{R}^3, \exists Z_H \in H$ such that $\Gamma(Z, Z_H) \leq \gamma_0$, where $\Gamma(Z_1, Z_2)$ is the distance in time-delay space

$$\Gamma(Z_1, Z_2) \triangleq \sqrt{\frac{1}{N_\psi} \sum_{\psi=1}^{N_\psi} (\tau^{\psi,Z_1} - \tau^{\psi,Z_2})^2} \quad (12)$$

and γ_0 is the desired precision in samples. Since we typically upsample $R_{\text{PHAT}}^\psi(\tau)$ with a factor α_{up} , the desired precision is set accordingly to $\gamma_0 = 1/\alpha_{up}$. The grid H is built by picking points heuristically on a few concentric spheres centered on the microphone array. The spheres' radii were also determined by γ_0 . Conceptually this approach relates to [16]. Note that in practice, the estimated range is imprecise, and only the azimuth and elevation are significant. Finally, for each time frame, our implementation approximates (11) by

$$\hat{Z} \approx \arg \max_{Z \in H} [P_{\text{SRP-PHAT}}(Z)]. \quad (13)$$

2) *Speech/Nonspeech Classification*: In the second step, a speech/nonspeech classification algorithm based on short-term clustering of the localization results is used to filter out noisy speaker location estimates. Conventional single-channel speech/nonspeech segmentation approaches are based upon energy, signal-to-noise ratio (SNR) estimation [9], or more complex estimators such as zero-crossing rate [30]. While relatively robust, techniques based on energy thresholding often miss low-energy beginnings of words and short speaker turns. Furthermore, they can provide a significant amount of erroneous audio estimates to the observation model. Unlike traditional approaches, we pose the problem of speech/nonspeech classification in the framework of localization, making decisions purely based on the location information. We first run single source localization on each time frame, then classify each

frame as speech or nonspeech, relying on short-term clustering of location estimates. Our motivation for short-term clustering is that noisy location estimates present high variations over time, while location estimates are consistent during speech periods. The algorithm has three steps: 1) build short-term clusters of frames whose location estimates are close to each other; 2) retain only significant clusters by applying a duration constraint; and 3) label those frames belonging to any significant cluster as speech, others as nonspeech.

In step 1), two frames t_1 and t_2 belong to the same cluster if $d(\hat{Z}_{t_1}, \hat{Z}_{t_2}) < d_0$ and $|t_2 - t_1| \leq T_0$, where d_0 and T_0 are thresholds in space and time, respectively. $d(\hat{Z}_{t_1}, \hat{Z}_{t_2})$ is a distance defined according to the setup. With a single, planar microphone array, it is reasonable to use the difference in azimuth between \hat{Z}_{t_1} and \hat{Z}_{t_2} . T_0 should be close to the length of a phoneme.

For step 2), we find the longest segment of contiguous frames within each cluster. If that segment lasts more than a threshold T_S , the cluster is kept as “significant,” otherwise it is dropped. Simpler criteria such as minimum cluster duration or the minimum number of frames within the cluster did not prove adequate. Additionally, to eliminate diffuse or minor far-field noise sources (e.g., PC), we also discard clusters whose mean square SRP-PHAT value is below a threshold $T_{\text{SRP-PHAT}}$.

In step 3), frames belonging to any significant cluster are labeled as speech, others as nonspeech. In the usual case where the audio frame rate is higher than the video frame rate, we down-sample the audio by grouping audio 3-D estimates between consecutive video frames. Specifically, in our work we define the audio and the video frame rates to be equal to 62.5 and 25 f/s, respectively (also see Section VIII-A), so there can be zero (nonspeech), one, two, or three (speech) audio 3-D estimates $\{\hat{Z}_t\}$ per video frame.

3) *AV Calibration*: Mapping the 3-D audio location estimates onto the camera image planes requires a form of sensor calibration. As discussed in Section II, most previous works have either assumed simplified configurations [3], [44] or resorted to rigorous camera calibration procedures [5], [6], [50]. Note that, in general, cameras and microphones might not necessarily remain in the same location for long term, so practical calibration procedures are needed to cope with sensor changes. Unlike such previous approaches, we use a nearest-neighbor approach to project 3-D audio estimates on the corresponding 2-D image planes, exploiting the fact that, although audio localization estimates can be noisy, and visual calibration is affected by geometric distortion, their joint occurrence tends to be more consistent. The procedure requires an offline, rough AV calibration procedure between the sensors, without requiring precise geometric calibration of audio and video. The procedure uses training data collected by having a person talking while performing activities in the meeting room in typical locations (walking, sitting, moving while seated, standing at the whiteboard and projector screen areas). The correspondences between 3-D and 2-D+camera-index vectors are obtained from the audio estimates as described earlier in this section, and from the output of a single-person PF-based visual tracker, respectively. For nonoverlapping fields-of-view (FOVs), the set of correspondences obtained from the training set defines a mapping between discrete sets $\Gamma : \mathbb{R}^3 \rightarrow \mathbb{R}^2 \times \{0, \dots, N_{\text{CAM}} - 1\}$, where

N_{CAM} is the number of cameras, such that 3-D locations are mapped into vectors containing 2-D image position (u_t, v_t) and camera index cam_t , $\Gamma(Z_t) = (u_t, v_t, \text{cam}_t)$. Note that when several image views are concatenated into a single image (as we do in Section VIII), the camera index simply results in a fixed 2-D translation term added to (u_t, v_t) . Finally, the mapping for unseen data is computed via nearest neighbor search.

The audio observation likelihood is finally defined on the image domain, relating the Euclidean distance between the 2-D audio location estimates and the candidate particles. For object i , let $x_{i,t}^a = (u_{i,t}^a, v_{i,t}^a)$ denote the audio estimate closest to the object’s translation components, $x_{i,t} = (u_{i,t}, v_{i,t})$. We then define a distribution for each value of the speaking activity variable

$$p(\mathbf{Y}_{i,t}^a | \mathbf{x}_{i,t}, k_{i,t} = 1) \propto \begin{cases} K_1^a, & \|x_{i,t} - x_{i,t}^a\| \leq \mathcal{R}^a \\ K_2^a, & \text{otherwise} \end{cases} \quad (14)$$

$$p(\mathbf{Y}_{i,t}^a | \mathbf{x}_{i,t}, k_{i,t} = 0) \propto \begin{cases} K_1^a, & \|x_{i,t} - x_{i,t}^a\| \geq \mathcal{R}^a \\ K_2^a, & \text{otherwise} \end{cases} \quad (15)$$

where \mathcal{R}^a defines a radius around the translation components of $\mathbf{X}_{i,t}$, and $K_1^a > K_2^a$ are constant terms introduced to reflect the desired situation: the likelihood of a person to be speaking must be large when there exists a nearby audio estimate, and small if such condition does not hold (e.g., $K_1^a/K_2^a = 10$). In case no audio location estimates exist, $u_{i,t}^a$ and $v_{i,t}^a$ are set to an arbitrarily large number.

B. Shape Observations

Assuming that shapes are embedded in clutter, edge-based observations are computed, based on Isard and Blake’s classic model [18], along L normal lines to a hypothesized elliptical contour. This results in a vector of C_l candidate positions for each line l , $\{z_{i,c}^l, l \in \{1, \dots, L\}, c \in \{1, \dots, C_l\}\}$, relative to $z_{i,0}^l$, the point lying on the contour. With some typical assumptions, the shape-based likelihood for each object is given by

$$p(\mathbf{Y}_{i,t}^{sh} | \mathbf{X}_{i,t}) \propto \prod_{l=1}^L \max \left(K^{sh}, \exp \left(-\frac{\|z_{i,\hat{c}}^l - z_{i,0}^l\|^2}{2(\sigma^{sh})^2} \right) \right) \quad (16)$$

where $z_{i,\hat{c}}^l$ is the position of the detected edge on line l that is closest to the elliptical contour, σ^{sh} is a standard deviation parameter, and K^{sh} is a constant that limits the influence of cases in which no edges are detected.

C. Spatial Structure Observations

We propose an observation model of the spatial structure of human heads, based on a parametric representation of the overlap between skin-blobs and head configurations. The model is based on the fact that the presence of skin pixels in a typical head blob is usually limited to specific regions inside and outside a head elliptical configuration (Fig. 1). Skin pixels are mainly distributed in the central and lower regions of a head, but also outside the head ellipse, e.g., on the neck region. Additionally, the skin-color blobs corresponding to a head often appear connected to other skin-color blobs due to body postures of people in conversations (e.g., resting the head on a hand).

Skin-color blobs are extracted at each frame according to a standard procedure. A 20-component Gaussian mixture model (GMM) of skin color in RGB space was estimated from a training set of people participating in real meetings in the multisensor meeting room described in Section VIII, including Caucasian, Indian, and Latin-American individuals, and collected over several days [31]. Skin pixels were classified based on thresholding of the skin likelihood, followed by morphological postprocessing to extract blobs (Fig. 1, center).

The spatial structure model is based on features of spatial overlap between skin-color blobs and candidate configurations, similar to the ones described in Section IV. Given a set of skin-color blobs and a single-object configuration $\mathbf{X}_{i,t}$, and assuming that the configuration is the reference, the recall ρ between the spatial support $\mathcal{S}_{i,t}$ and each blob is computed. Let $\mathcal{S}_{i,t}^B$ denote the spatial support of the blob with the largest recall. A head template is further decomposed into three nonoverlapping parts with spatial support $\mathcal{S}_{i,t}^l$, $l \in \{1, 2, 3\}$, $\mathcal{S}_{i,t} = \cup_l \mathcal{S}_{i,t}^l$ (Fig. 1, right). With this representation, the overlap measures first defined in (6), i.e., precision and recall, are computed for each of the head parts $\nu(\mathcal{S}_{i,t}^l, \mathcal{S}_{i,t}^B)$ and $\rho(\mathcal{S}_{i,t}^l, \mathcal{S}_{i,t}^B)$, and for the whole head, $(\nu(\mathcal{S}_{i,t}, \mathcal{S}_{i,t}^B)$ and $\rho(\mathcal{S}_{i,t}, \mathcal{S}_{i,t}^B)$). Although the proposed features are obviously not as discriminant as the ones used in dedicated face processing algorithms (e.g., [45]), they perform reasonably well in realistic conditions, including out of plane rotation, and partial occlusion. The features define an eight-component observation space $\mathbf{Y}_{i,t}^{st}$. The spatial structure observation model is finally represented by a mixture model composed of a GMM with diagonal covariance matrices, and a uniform distribution $U(\cdot)$ used to limit the effect of very low likelihood values

$$p(\mathbf{Y}_{i,t}^{st}|\mathbf{X}_{i,t}) \propto \omega_0 U(\mathbf{Y}_{i,t}^{st}) + \sum_{l=1}^{N_{st}} \omega_l \mathcal{N}(\mathbf{Y}_{i,t}^{st}, \mu_l, \Sigma_l) \quad (17)$$

where $\{\omega_0, \omega_l, \mu_l, \Sigma_l\}$ are model parameters. When no blobs are detected, the likelihood is set to a constant value.

VI. MCMC SAMPLING

Inference with a traditional particle filter (based on importance sampling) on the high-dimensional space defined by several objects being tracked is computationally infeasible, given that the number of particles required for a given performance grows roughly exponentially with the dimensionality of the space [11], [29]. In order to efficiently place samples as close as possible to regions of high likelihood, we build on the recent work of Khan *et al.* [22] and approximate (4) with MCMC techniques, using a Metropolis–Hastings (MH) sampler at each time-step. MCMC methods produce a sequence of samples from a Markov chain whose stationary distribution corresponds to the target distribution (the filtering distribution in the tracking case), after running the sampler long enough, and discarding the initial part of the run, called burn-in period [29]. The MH algorithm consists of two iterative steps. First, given a current configuration \mathbf{X} , a new sample \mathbf{X}^* is drawn from a proposal distribution $q(\mathbf{X}^*|\mathbf{X})$. Then, the proposed

sample is accepted as the new configuration in the Markov chain with probability (also called acceptance ratio)

$$\alpha = \min\left(1, \frac{p(\mathbf{X}^*)q(\mathbf{X}|\mathbf{X}^*)}{p(\mathbf{X})q(\mathbf{X}^*|\mathbf{X})}\right) \quad (18)$$

where $p(\mathbf{X})$ denotes the target distribution (in our case $p(\mathbf{X}) = p(\mathbf{X}_t|\mathbf{Y}_{1:t})$). If the move is not accepted, the chain remains in the same configuration. The sample set obtained by the MH sampler is a fair sample from the true filtering distribution, and so all particle weights are equal to $1/N$ [29].

In the tracking case, we run a MH sampler at each time-step. However, for computational tractability, a proposal distribution that simplifies the evaluation of the acceptance ratio is needed, as (18) involves the evaluation of (4) (a sum over all particles). We define a mixture model over all objects, where one object is chosen at each step in the chain to attempt a move

$$q(\mathbf{X}_t^*|\mathbf{X}_t) = \sum_i q(i)q(\mathbf{X}_t^*|\mathbf{X}_t, i) \quad (19)$$

where $q(i)$ is the prior over object indices, and $q(\mathbf{X}_t^*|\mathbf{X}_t, i)$ are the mixture components. To construct a candidate configuration \mathbf{X}_t^* from the current configuration \mathbf{X}_t , an object index i^* is first chosen with probability $q(i = i^*)$. A move will be attempted on i^* , while the rest of the multiobject configuration is left unchanged. The mixture components are defined so that

$$q(\mathbf{X}_t^*|\mathbf{X}_t, i) \propto \begin{cases} \frac{1}{N} \sum_n p(\mathbf{X}_t^*|\mathbf{X}_{t-1}^{(n)}), & i = i^* \\ \frac{1}{N} \sum_n p(\mathbf{X}_t^*|\mathbf{X}_{t-1}^{(n)}), & i \neq i^*, \mathbf{X}_t^* = \mathbf{X}_t \\ 0, & i \neq i^*, \mathbf{X}_t^* \neq \mathbf{X}_t \end{cases} \quad (20)$$

which implies that given i^* , the new configuration for object i^* is sampled from $p(\mathbf{X}_{i^*,t}^*|\mathbf{X}_{i^*,t-1}^{(n^*)})$, using a particle n^* sampled from the particle set of the previous time-step, while keeping all the other object configurations fixed. Using the Dirac delta function, the specific expression fulfilling (20) is

$$q(\mathbf{X}_t^*|\mathbf{X}_t, i) = \frac{1}{N} \sum_n p(\mathbf{X}_{i^*,t}^*|\mathbf{X}_{i^*,t-1}^{(n)}) \cdot \prod_{l \in \mathcal{I}_t - \{i\}} p(\mathbf{X}_{l,t}|\mathbf{X}_{l,t-1}^{(n)}) \delta(\mathbf{X}_{l,t}^* - \mathbf{X}_{l,t}). \quad (21)$$

This distribution fulfills the desired property of canceling out all the factors that involve summations over particles in the acceptance ratio. It is not difficult to show that the acceptance probability is simplified to

$$\alpha = \min\left(1, \frac{p(\mathbf{Y}_t|\mathbf{X}_t^*) \prod_{(i^*,j) \in \mathcal{C}_{i^*}} \phi(\mathbf{X}_{i^*,t}^*, \mathbf{X}_{j,t}^*)}{p(\mathbf{Y}_t|\mathbf{X}_t) \prod_{(i^*,j) \in \mathcal{C}_{i^*}} \phi(\mathbf{X}_{i^*,t}, \mathbf{X}_{j,t})}\right) \quad (22)$$

where \mathcal{C}_{i^*} denotes the set of pairwise cliques that involve object i^* . For the factorized form for the multiobject observation likelihood (8), the expression can be further simplified to

$$\alpha = \min\left(1, \frac{p(\mathbf{Y}_{i^*,t}|\mathbf{X}_{i^*,t}^*) \prod_{(i^*,j) \in \mathcal{C}_{i^*}} \phi(\mathbf{X}_{i^*,t}^*, \mathbf{X}_{j,t}^*)}{p(\mathbf{Y}_{i^*,t}|\mathbf{X}_{i^*,t}) \prod_{(i^*,j) \in \mathcal{C}_{i^*}} \phi(\mathbf{X}_{i^*,t}, \mathbf{X}_{j,t})}\right) \quad (23)$$

Generate N samples $\{\mathbf{X}_t^{(n)}, w_t^{(n)}\}$ from $\{\mathbf{X}_{t-1}^{(n)}, w_{t-1}^{(n)}\}$.

- Initialize the MH sampler, by sampling \mathbf{X} from the purely predictive distribution $\sum_n w_{t-1}^{(n)} \prod_{i \in \mathcal{I}_t} p(\mathbf{X}_{i,t} | \mathbf{X}_{i,t-1}^{(n)})$. This implies (a) sampling a particle n^* from the particle set obtained at the previous time-step, $\{\mathbf{X}_{t-1}^{(n)}, w_{t-1}^{(n)}\}$, and (b) use this particle to sample from the distribution $\prod_{i \in \mathcal{I}_t} p(\mathbf{X}_{i,t} | \mathbf{X}_{i,t-1}^{(n^*)})$, which predicts the state of each object based on the factorized dynamical model.
- MH sampling. Draw $B + N$ samples, where B and N denote the number of particles in the burn-in and fair sample sets, respectively. For each sample,
 - Sample \mathbf{X}^* from $q(\mathbf{X}^* | \mathbf{X})$ using Eq. 19. This involves (a) choosing an object index i^* sampling from $q(i)$, and (b) sampling a particle from the distribution specified in Eq. 21, which changes the configuration of only one object at a time.
 - Compute acceptance ratio α using Eq. 23. This involves the evaluation of (1) the single-object AV observation likelihood for the object indexed by i^* (Eqs. 8, 14, 15, 16, and 17), and (2) the MRF term involving all pairwise potentials involving the object indexed by i^* , for both the current configuration and the proposed move.
 - Accept \mathbf{X}^* , i.e., assign the proposed move \mathbf{X}^* to the current configuration \mathbf{X} ($\mathbf{X} \leftarrow \mathbf{X}^*$), with probability α . If the move is not accepted, the chain remains in the current value for \mathbf{X} .
 - Add \mathbf{X} to the set of particles for the current time-step, $\{\mathbf{X}_t^{(n)}, w_t^{(n)}\}$, with $w_t^{(n)} = 1/N$. This set will receive a new particle at each step in the chain.
- Compute mean estimate $\hat{\mathbf{X}}_t$ using Eq. 24, determining first the discrete component, and then the continuous component for each object.

Fig. 2. MCMC PF algorithm for AV multispeaker tracking.

which only involves the evaluation of single-object AV likelihood terms. With this definition, the MH sampler improves the prediction of multiobject configurations by accepting, at each step, single-object candidates that are closer to a region of high likelihood, without discarding good candidates already accepted for other objects.

Once a set of particles has been generated, the mean estimate is approximated by the marginal mean estimates for each object, $\hat{\mathbf{X}}_t = (\hat{\mathbf{X}}_{i,t})$, $i \in \mathcal{I}_t$. Each $\hat{\mathbf{X}}_{i,t}$ is computed as usual in mixed-state models, first computing the maximum *a posteriori* (MAP) estimate for the discrete variable $k_{i,t}$, and then the weighted mean of the continuous component $\mathbf{x}_{i,t}$ given the MAP discrete estimate [19]

$$\hat{k}_{i,t} = \arg \max_m \sum_{n \in \mathcal{J}_{i,m}} w_t^{(n)}; \quad \hat{\mathbf{x}}_{i,t} = \frac{\sum_{n \in \mathcal{J}_{i,\hat{k}_{i,t}}} w_t^{(n)} \mathbf{x}_{i,t}^{(n)}}{\sum_{n \in \mathcal{J}_{i,\hat{k}_{i,t}}} w_t^{(n)}} \quad (24)$$

where $\mathcal{J}_{i,m} = \{n | k_{i,t}^{(n)} = m\}$. The full MCMC-PF algorithm is summarized in Fig. 2.

Other formulations combining MCMC iterations with PF techniques exist in the statistics literature [4], [12], [15], [28], all with the goal of overcoming the limitations of the importance sampling technique that is at the core of the basic PF. When the particles store the complete temporal trajectories of the states, the resample-move algorithm by Gilks and Berzuini [15] combines a resample step (importance-weighted resampling) and a move step (one or more MCMC iterations on each particle

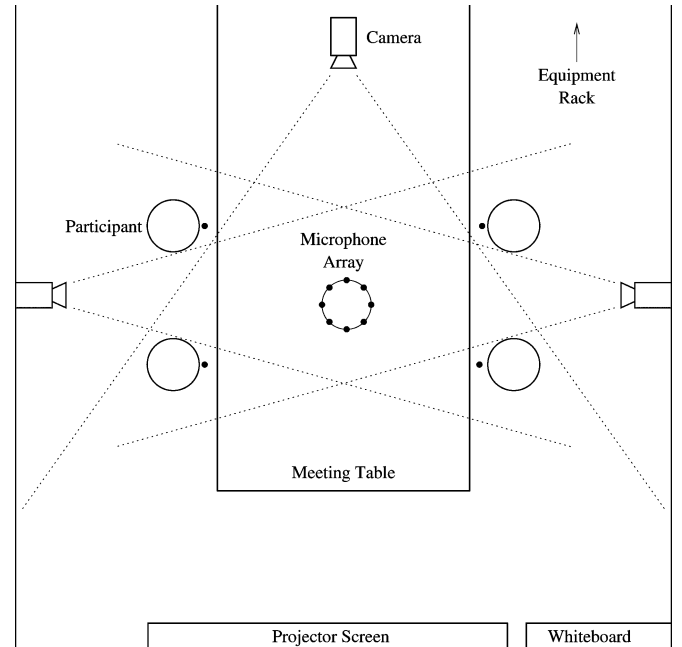


Fig. 3. Meeting recording configuration.

selected at the resample step) to increase particle diversity. As an improvement to this scheme, Fearnhead [12] proposes to introduce MCMC moves in a PF when only summaries of

the trajectories of each particle, derived from sufficient statistics of the state parameters, are kept, which reduces storage requirements. As pointed out by Khan *et al.* [22], the MCMC algorithm used here could be regarded as a particular case of the work by Berzuini *et al.* [4], using a posterior distribution that includes the MRF prior term, and a specific proposal distribution designed to handle the multiobject case. An alternative view of [4] is presented by Liu and Chen [28].

VII. VARYING NUMBER OF PEOPLE

Although the MCMC-PF could formally integrate birth-death processes as part of the filtering recursion (e.g., via reversible-jump MCMC [29]), this would require a multiperson observation model that allowed for the comparison between configurations containing varying number of people [5], [20]. The factorized observation model in (8) is not suitable for such a case. For this reason, we opted for a simple process in which, at each time frame, the set of people of the scene \mathcal{I}_t is first established, and then the MCMC-PF is applied on the detected \mathcal{I}_t . It has been argued in the past (e.g., by Perez *et al.* [36]) that, unless a clear ambiguity in the number of scene objects exists, the detection-then-tracking mechanism can be more efficient than the case in which particles with varying number of objects coexist in the same time-step, as particles corresponding to the “wrong” number of objects are effectively wasted.

New objects are handled as follows. All skin-color blobs inside a set of birth-likely scene regions, and not overlapping with existing objects, are probed as candidates. Given a standard ellipse template, and a new object ID i^* (chosen as the next available object ID in a list), a number of single-object samples $\{\mathbf{X}_{i^*,t}^{(r)}\}$ is constructed by drawing samples $\{\mathbf{x}_{i^*,t}^{(r)}\}$ from a Gaussian distribution (with mean translation equal to the blob centroid, mean scaling set to unity, and diagonal covariance matrix set to explore a relatively short space around the mean), while setting $\{k_{i^*,t}^{(r)}\}$ to zero. The set of samples is ranked based on their visual likelihood, $p(\mathbf{Y}_{i^*,t}^{sh}|\mathbf{X}_{i^*,t})p(\mathbf{Y}_{i^*,t}^{st}|\mathbf{X}_{i^*,t})$, and the presence of a new object is decided by thresholding the likelihood of the best configuration. This best configuration is then used in the prior in the MCMC-PF for the new object. Needless to say, more robust people detectors could be integrated in our approach [45]. Object disappearance is declared whenever a configuration leaves the image limits, or when a configuration has too low visual likelihood. Finally, continuing people are handled as in the case of fixed number of objects.

VIII. EXPERIMENTS AND RESULTS

A. Data Collection

Data are recorded in a $8.2 \times 3.6 \times 2.4$ m meeting room containing a 4.8×1.2 m rectangular meeting table, and equipped with fully synchronized video and audio capture devices (Fig. 3). The video equipment includes three identical uncalibrated CCTV cameras [34]. Two cameras on opposite walls record frontal views of participants, including the table and workspace area, and have nonoverlapping fields-of-view.

A third wide-view camera looks over the top of the participants towards the white-board and projector screen. The audio equipment consists of an eight-element circular equi-spaced microphone array centered on the table, with diameter 20 cm, and composed of high-quality miniature electret microphones. Video was recorded at 25 Hz, with an image size of 288×360 pixels. In our work, we define the duration of a time-step to be equal to 1/25 s. Therefore, video observations were computed for each available video frame. Audio was recorded at 16 kHz. As described in Section V-A, audio observations were first computed at 62.5 f/s, and then merged with the video features to define the audiovisual observations. Training data to estimate the GMM parameters for skin-color models and spatial structure features, and for the AV calibration procedure, were additionally recorded in the meeting room. In Section VIII-D, we present results on two two-camera sequences, (*meeting1* and *meeting2*, 1715 and 1200 video frames, respectively), and one three-camera sequence (*meeting3*, 1200 video frames). The sequences are composed by concatenating the different views into one larger merged image. The first two sequences have nonoverlapping fields-of-view, while in the third there is some overlap.

B. Parameter Setting

For the audio source localization algorithm, we used $\alpha_{up} = 20$. The thresholds in the speech/nonspeech classification algorithm were set to $d_0 = 5^\circ$, $T_0 = 200$ ms, $T_S = 100$ ms, and $T_{SRP-PHAT} = 0.03$. Following our previous work [14], the first two thresholds were intuitively chosen, based on experiments conducted on a separate test data set, and on the typical phoneme length, respectively. The third threshold was chosen on a single, separate test case. Regarding the video observations, the GMM parameters for skin-color pixels and spatial structure features were estimated by standard expectation maximization (EM). Model selection was automatically done using the minimum description length principle. All other parameters were set by hand to sensible values, and kept fixed for all experiments. Regarding the dynamical model for the single-object continuous dynamics $p(\mathbf{x}_{i,t}|\mathbf{x}_{i,t-1})$, we use an augmented continuous state, $\tilde{\mathbf{x}}_{i,t} = (\mathbf{x}_{i,t}, \mathbf{x}_{i,t-1})$, and express the dynamics as $\tilde{\mathbf{x}}_{i,t} = A\tilde{\mathbf{x}}_{i,t-1} + B(\omega_t, 0)^T$, with

$$A = \begin{bmatrix} 2 & -1 \\ 1 & 0 \end{bmatrix}, \quad B = \begin{bmatrix} 1 & 0 \\ 0 & 0 \end{bmatrix}$$

and ω_t is a white noise process with standard deviations for translation and scaling equal to 4 and 10^{-4} , respectively. The TPM parameters for speaking activity were set to $\beta_{00} = \beta_{11} = 0.8$, $\beta_{01} = \beta_{10} = 0.2$. For the interaction model, $\lambda_\phi = 3$. In the audio observation model, $R^a = 50$ pixels, and $K_1^a = 1 = 10K_2^a$. For the shape-based observations, the number of measurement lines $L = 16$, each with length $a = 20$ pixels, $\sigma^{sh} = 5$, and $K^{sh} = \exp(-((a/2)^2/2(\sigma^{sh})^2)) = e^{-2}$. A scaling procedure was applied as the various likelihood terms have a different dynamic range. Finally, we assume a uniform prior for the proposal $q(i)$ in the MH sampler.

C. Performance Evaluation Measures

We evaluate both the tracking quality and the ability to infer speaking activity. The first criterion is evaluated based on the degree of matching between the ground truth (GT) and the tracker estimates. For this purpose, a semiautomatic head bounding-box GT is first generated for each person at each video frame, using the color-based single-person tracker proposed by Perez *et al.* [36]. Then, for each person and for each frame, the precision/recall overlap measures defined in (6) are computed between the tracker estimates (represented by the bounding box that encloses the spatial support of the mean estimate) and the GT, assuming that the latter is the reference. The overlap measures are used to define four person-based measures.

- 1) *Track state (TS)*. A frame-level binary variable, which is unity if both precision and recall are greater than a threshold T_{TS} , and zero otherwise. In the experiments, $T_{TS} = 0$.
- 2) *Track F-measure (F_T)*. The precision/recall combination ($F_T = 2\nu\rho/(\nu + \rho)$) is computed for those frames with $TS = 1$.
- 3) *Success rate (SR)*. A sequence-level variable, defined as unity if $TS = 1$ for the entire sequence, and zero otherwise.
- 4) *Tracking rate (TR)*. A sequence-level variable, defined as the ratio between the number of frames where $TS = 1$ and the number of frames in the sequence.

Jointly, F_T , SR , and TR provide an indication of the quality and stability of the tracker, including eventual recovery from failures. Note that SR is a much stricter measure than TR . All results are computed over multiple runs of the particle filter, to account for its stochastic nature. SR and TR are then reported as averages. Finally, an overall average over all people in the sequence is also reported. For all these measures, the standard deviation computed over all people in the sequence is additionally indicated.

Regarding speaking activity, a binary GT of speaker turns was manually generated for each person. For these 1-D sets, precision and recall are then computed between the GT and the tracker estimate of speaking activity for each person, defining:

- 5) *Speaking status F-measure (F_S)*. For each person, a measure computed as in F_T .

Finally, F_S is also reported as averages over multiple runs and people, as with the other measures.

D. Results and Discussion

We now present and discuss the results obtained for each individual sequence, and conclude with an overall discussion at the end of this section. First, we evaluated the specific abilities of our framework to estimate location and speaking activity, conducting experiments under two controlled conditions: 1) the number of tracked people was known and kept fixed for the duration of the sequence, and 2) the tracker was hand-initialized in the first frame. The source localization algorithm was originally evaluated in [14]. Details of such evaluation are not included here for space reasons, but in summary, the objective evaluation of the short-term clustering algorithm confirmed its superiority

over energy-based methods for the speech detection task, as further developed in [25]. Second, we evaluated the performance of the algorithm handling varying numbers of objects; the results are discussed towards the end of this section.

In all cases, the estimated mean configuration is displayed, at each time-step for each person, as an ellipse of distinct color. The inferred speaking activity is shown as a double ellipse with contrasting tones. The number of particles in all cases was $B + N = 500$, with 30% of the particles being discarded in the burn-in period of the MH sampler. All the results were obtained using 20 runs of the MCMC-PF. People are given an object identifier (O_1, O_2, \dots) with respect to the position they first occupy in the video, from left to right. The overall average and standard deviation computed over the number of people in the sequence (O_{avg} and $\sigma_{O_{\text{avg}}}$, respectively) are reported in results in all cases. The results are best appreciated by watching the videos at the companion website: <http://www.idiap.ch/~gatica/av-tracking-multiperson.html>.

1) *Meeting1*: The results on the *meeting1* sequence are shown in Fig. 4 and Table I. In this sequence, recorded with no visual background clutter, four seated speakers are engaged in a conversation and talk at a relaxed pace, taking turns with little overlap, which occurs for instance when people laugh. The last row in Table I (S_{GT}) indicates the proportion of time during which each person spoke in the sequence, as labeled in the speaking activity GT.

Regarding visual tracking with our approach, the four objects were tracked with good quality and stably throughout the sequence for all runs (see SR , TR , and F_T rows in Table I, and video `meeting1_mcmc_500.avi` on the website). The algorithm can handle partial self-occlusion and variations of head pose (from frontal to side views), which confirms the advantages of combining visual cues. With respect to speaking activity, our source localization method has shown to be able to estimate location reasonably well, and detect speaker turns with good accuracy and low latency. The audio activity inferred by the MCMC-PF preserves these properties for those segments where only one speaker takes the turn, while smoothing out very short speaker turns (see F_S row in Table I). Although we use a single-source localization algorithm, the MCMC-PF can sometimes infer simultaneous speaking activity for multiple participants [Fig. 4(a)]. In general, however, a “dominant speaker” effect is observed in overlapping speech segments.

To validate the efficiency of the MCMC-PF, we compare it with a traditional joint multiobject PF, which uses importance sampling instead of MCMC, while all other aspects and parameters of the filter remain fixed. Results are also computed using 20 runs, and are shown in Table I, Fig. 4(d), (e), and video `meeting1_pf_500.avi`. Clearly, our approach outperforms the traditional PF in both ability to track and estimation of the speaking activity. With the classic PF, a loss of track occurred for all of the objects (see SR) at some point in the sequence (especially poor for O_2 , who was tracked successfully only in 60% of the runs). The tracker also has high visual jitter. Furthermore, the inference of speaking activity is degraded considerably. The performance loss is explained by the way in which the multiobject state-space is explored in a traditional joint PF. Many particles are effectively wasted: a poor



Fig. 4. Multispeaker tracking results, *meeting1*. Both location and speaking activity (double ellipse if a person speaks) are inferred for each participant. (a–c): MCMC-PF, images correspond to frames 526, 1120, and 1420, respectively. (d), (e): traditional PF: images correspond to frames 905 and 910, respectively. Tracking is lost for O1 for the rest of the sequence.

candidate configuration for one object will produce a low multi-object likelihood value, even though the candidates for all other objects might be well placed. Additionally, relatively poor geometric configurations combined with correct speaking activity values might be common, given the joint audiovisual observation model. A combination of these factors with, e.g., motion changes might eventually drift one or more objects away from the correct configuration and result in tracking loss [Fig. 4(e)]. A standard proportion test indicates that the difference in performance between MCMC-PF and PF for O_{avg} is statistically significant with confidence greater than 99.99% for both SR and TR . As a final remark, the number of particles that is required

TABLE I
TRACKING RESULTS FOR *meeting1*, FOR OUR APPROACH AND A TRADITIONAL MULTI-OBJECT PF. RESULTS ARE SHOWN FOR INDIVIDUAL PEOPLE, AND AVERAGED OVER ALL PEOPLE

<i>method</i>	<i>measure</i>	O1	O2	O3	O4	O_{avg}	$\sigma_{O_{avg}}$
MCMC-PF	SR	1.00	1.00	1.00	1.00	1.00	0.00
	TR	1.00	1.00	1.00	1.00	1.00	0.00
	F_T	0.89	0.87	0.85	0.92	0.88	0.03
	F_S	0.71	0.75	0.77	0.75	0.75	0.03
PF	SR	0.80	0.60	0.85	0.90	0.79	0.13
	TR	0.95	0.79	0.94	0.98	0.92	0.09
	F_T	0.87	0.86	0.83	0.87	0.86	0.02
	F_S	0.60	0.62	0.55	0.61	0.59	0.03
	S_{GT}	0.19	0.19	0.10	0.16	0.16	0.04

with the traditional PF to perform as well as the MCMC-PF is prohibitively high. These results also confirm those obtained by Khan *et al.* [22] where, for a quite different tracking scenario (visual tracking of ants), it was also found that an MCMC-PF outperforms a basic PF.

2) *Meeting2*: The results on the *meeting2* sequence are shown in Fig. 5, Table II, and in the video *meeting2_mcmc_500.avi*. This sequence depicts four seated speakers in a more animated conversation (see S_{GT} row in Table II), with many turns and cases of overlapping speech. There are also two sources of visual clutter: the textured background, and a fifth walking person (not tracked) who enters and leaves the scene creating visual distraction by approaching the speakers. Our algorithm performs quite satisfactorily with respect to quality of tracking and speaker activity detection. Although the tracker gets momentarily distracted by the walking person or the background, it recovers in almost all cases, as shown by the SR , TR , and F_T rows in Table II. The combination of visual cues renders the tracker more robust: on one hand, the spatial structure observations help in cases of uncertainty with respect to edge information (e.g., textured background). On the other hand, the shape observations refine the spatial structure model, which consistently drives the tracker to skin-blob areas, but sometimes without much accuracy. A limitation of the likelihood model can be seen for O3 in Fig. 5(a)–(c), where the ellipse-to-head fitting is less precise. Finally, our approach is again significantly more effective than a traditional joint multi-object PF, which in this case shows an even more severe performance degradation (see Fig. 5(d), (e), Table II, and video *meeting2_pf_500.avi*). The traditional PF is unable to track all of the objects consistently, the quality of the estimation of speaking activity is considerably degraded, and most figures are considerably lower than the ones obtained for *meeting1*. The standard proportion test shows a statistically significant difference in performance between MCMC-PF and PF for O_{avg} , with confidence greater than 99.99%, for both SR and TR . Overall, these results suggest that the MCMC-PF is more robust to realistic conditions than the traditional approach.

Fig. 6 presents the results regarding speaking activity detection for each person as a function of the video frame number. In



Fig. 5. Multispeaker tracking results, *meeting2*. (a–c): MCMC-PF, images correspond to frames 360, 575, and 909, respectively. (d), (e): traditional PF: images correspond to frames 195 and 200, respectively. Tracking is lost for O2 and O4 for the rest of the sequence.

the first place, we display the results obtained with the audio-source localization algorithm mapped onto the image plane, assuming that the location of the meeting participants is known in the GT, i.e., dividing the image into four regions, manually assigning regions to people, and associating speaking activity estimates to individuals based on the region the estimates fall into (labeled as A in Fig. 6). We also present the results for our approach (labeled as AV), where the results correspond to the median of the inferred speaking activity estimated over 20 runs of the MCMC-PF. We finally display the manually labeled GT. Two cases are displayed, for different values of the parameters of the symmetric TPM: $\beta_{00} = 0.8$, $\beta_{01} = 0.2$ [Fig. 6(a)–(d)], and $\beta_{00} = 0.95$, $\beta_{01} = 0.05$ [Fig. 6(e)–(h)]. We first observe

TABLE II
TRACKING RESULTS FOR *meeting2*, FOR OUR APPROACH
AND A TRADITIONAL MULTIOBJECT PF

<i>method</i>	<i>measure</i>	O1	O2	O3	O4	O_{avg}	$\sigma_{O_{avg}}$
MCMC-PF	SR	0.95	0.95	1.00	1.00	0.98	0.03
	TR	0.99	0.97	1.00	1.00	0.99	0.01
	F_T	0.88	0.88	0.87	0.86	0.87	0.01
	F_S	0.72	0.72	0.71	0.79	0.74	0.04
PF	SR	0.60	0.40	0.35	0.75	0.52	0.18
	TR	0.68	0.45	0.50	0.79	0.61	0.16
	F_T	0.86	0.85	0.81	0.85	0.84	0.02
	F_S	0.55	0.38	0.42	0.65	0.50	0.12
	S_{GT}	0.26	0.24	0.19	0.35	0.26	0.07

that the source localization algorithm detects speak/nonspeak changes with low delay, and classifies most of the correct location estimates as speech frames. Furthermore, given the lack of a temporal smoothness constraint, long speaker turns are often broken into smaller turns. We also observe that short spurious turns due to noise are sometimes detected and incorrectly assigned to speakers. In contrast, the MCMC-PF introduces a temporal dynamical process that generates a smoothing effect. Short turns are often eliminated, which also tends to merge broken turns into longer units. The degree of smoothness clearly depends on the TPM parameters and their relation to the parameters in the switching audio observation likelihood (14), (15). As expected, the filtering is higher in Fig. 6(e)–(h) compared to Fig. 6(a)–(d). However, the larger the smoothing effect, the longer the delay to detect the initial and final parts of speaker turns, and this tradeoff needs to be taken into account in practice.

3) *Effect of the MRF Prior*: The influence of the MRF prior cannot be appreciated in the previous two cases because people do not occlude each other. To analyze the effect of this term, we conducted experiments with a five-person tracker on two excerpts of *meeting2*, where the walking silent person (O5) is significantly occluded by two seated participants several times. The first excerpt (*meeting2-oc1*) is 140 frames long (frames 550–690). The second one (*meeting2-oc2*) is 170 frames long (frames 830–1000). Performance is computed over 20 runs of the MCMC-PF, without and with the MRF prior.

Results for *meeting2-oc1* are shown in Table III, Fig. 7, and videos *meeting2_o1_mcmc_500_no_int.avi* (without MRF) and *meeting2_o1_mcmc_500_int.avi* (with MRF). Without the MRF prior, tracking is of high quality for objects O2–O4 ($SR = 1$, $TR = 1$, and $F_T \geq 0.87$, results not included in Table III for space reasons). The results for O1 and O5 are shown in Table III. For O1, tracking was lost once in 20 runs, locking onto O5. More importantly, for O5, tracking was lost in 25% of the cases. In contrast, the MRF prior produced very high quality tracking for the five objects ($SR = 1$, $TR = 1$, $F_T \geq 0.87$ for O2–O4, see Table III for O1 and O5).

For *meeting2-oc2*, the results are also shown in Table III. In this case, the occlusion affects objects O3 and O5, which got lost or confused with each other in a few runs. As can be

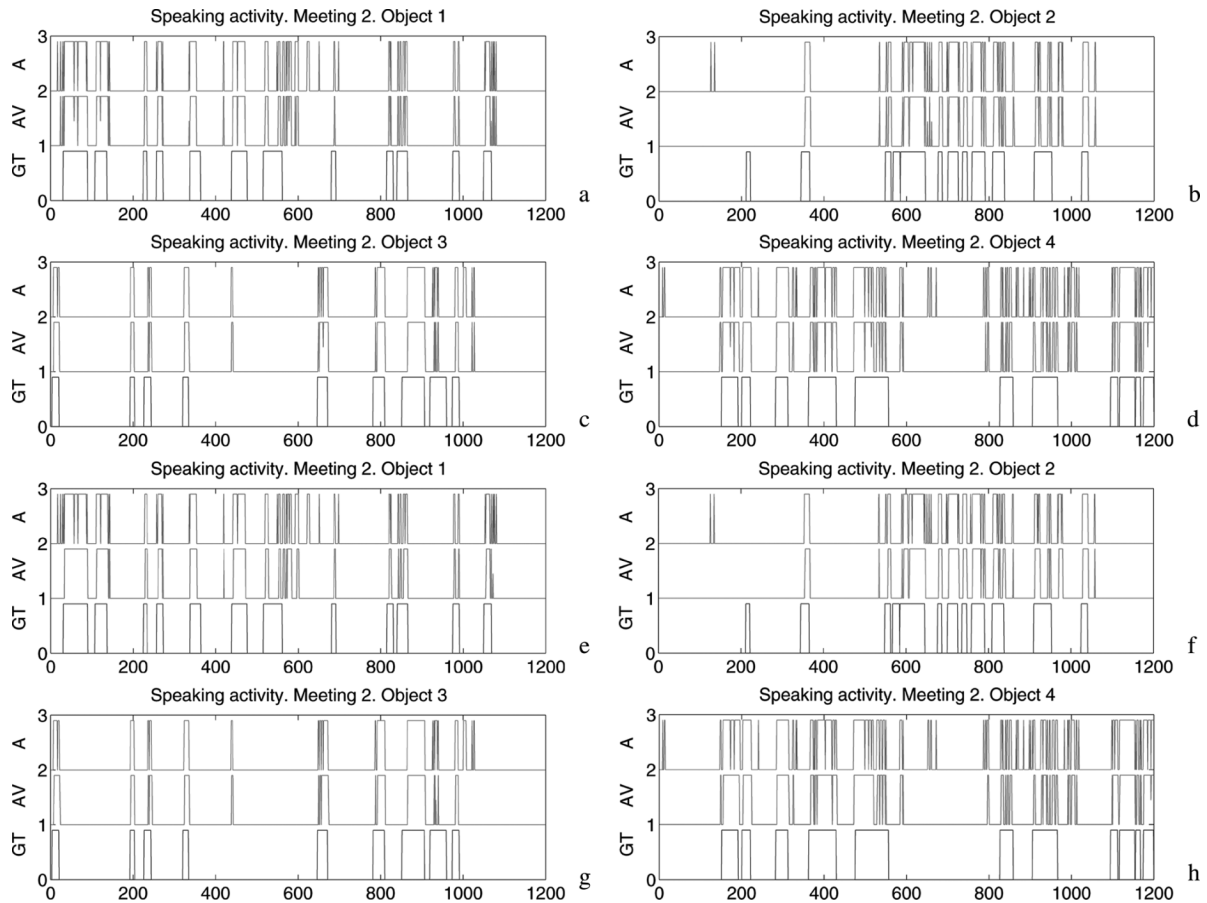


Fig. 6. Speaker activity inference results, *meeting2*. In each figure, results are shown, as a function of frame number, for audio + av mapping (A), the MCMC-PF approach (AV), and the manual ground truth (GT). Figures (a–d) correspond to O1–O4, respectively, for TPM values $\{0.8,0.2\}$. Figures (e–h) are the corresponding results for TPM values $\{0.95,0.05\}$.

TABLE III
RESULTS FOR SEQUENCES WITH PERSON OCCLUSION. PERFORMANCE WAS AFFECTED FOR O1 AND O5 IN *meeting2-oc1*, AND FOR O3 AND O5 IN *meeting2-oc2*. WO/W INDICATES WITHOUT/WITH MRF PRIOR

measure	<i>meet2-oc1</i>				<i>meet2-oc2</i>			
	O1wo	O5wo	O1w	O5w	O3wo	O5wo	O3w	O5w
SR	0.95	0.75	1.00	1.00	0.90	0.95	0.90	1.00
TR	0.96	0.89	1.00	1.00	0.92	0.96	0.92	1.00
F_T	0.87	0.74	0.88	0.74	0.77	0.72	0.76	0.74

seen from the table, the use of the interaction term brings an improvement for O5 without degrading the performance for O3. The performance for the other three objects (O1, O2, and O4) is of very high quality ($SR = TR = 1$, $F_T \geq 0.87$). An example video with the MRF prior can be seen in video *meeting2_o2_mcmc_500_int.avi*.

4) *Meeting3*: Results for this sequence are shown in Table IV, Fig. 8, and video *meeting3_mcmc_500.avi*. In this case, a person (O3) makes a presentation and uses the whiteboard, while the others remain seated and mostly silent (see S_{GT} row in Table IV). Our algorithm correctly tracks the location of the four people across the sequence, although tracking is more challenging for the presenter due to his size and distance from the array. As one would expect, the audio

localization algorithm detects a speaker at the table better than at a whiteboard/presentation, given the shorter distance to the microphone array. Due to this, when the presenter and a seated person speak simultaneously [Fig. 8(c)], the tracker infers speaking activity only for the person at the table. Additionally, when people clearly face away from the array, the audio estimates degrade, and so does the inference of the speaking status. Overall, the speaking activity of the presenter is inferred with reasonable quality, although some of his turns are missed [Fig. 8(e)]. The speaking activity of O1 and O4 is estimated with good quality, comparable to the obtained with the previous sequences. The comparatively low F_S -value for O2 is explained by the fact that he spoke briefly only once, and made noise that was identified as speaking activity. In comparison, as can be seen from Table IV and video *meeting3_pf_500.avi*, a traditional joint PF shows again a more degraded performance. The standard proportion test indicates a statistically significant difference between MCMC-PF and PF for O_{avg} , with confidence greater than 99.99%, for both SR and TR .

5) *Auto-Initialization*: A first example is shown in Fig. 9(a)–(c) and *meeting1_mcmc_500_autoinit.avi*. The tracker is initialized at frame 0 with $\mathcal{I}_0 = \emptyset$ (zero objects). The birth-likely area for this example is the entire scene, roughly above the chest of the seated participants. At frame 1, O1, O2, and O4 are automatically initialized, while O3 is initialized



Fig. 7. Five-object tracker, effects of the MRF model. (a–c): *meeting2-oc1*, frames 560, 585, and 594, without MRF prior. (d–f): same frames, with MRF prior.

once he moves his hand away from his face at frame 24. From this frame on, the performance is equivalent to the one obtained with manually initialized objects. A second example is shown in Fig. 9(d)–(f) and video *meeting2_mcmc_500_autoinit.avi*. In this case, the tracker is initialized at frame

TABLE IV
TRACKING RESULTS FOR *meeting3* FOR OUR APPROACH
AND A TRADITIONAL MULTIOBJECT PF

<i>method</i>	<i>measure</i>	O1	O2	O3	O4	O_{avg}	$\sigma_{O_{avg}}$
MCMC-PF	SR	1.00	1.00	1.00	1.00	1.00	0.00
	TR	1.00	1.00	1.00	1.00	1.00	0.00
	F_T	0.88	0.88	0.87	0.90	0.88	0.01
	F_S	0.81	0.57	0.57	0.79	0.69	0.13
PF	SR	0.95	0.15	0.45	0.95	0.62	0.39
	TR	0.95	0.27	0.87	0.96	0.76	0.33
	F_T	0.87	0.83	0.84	0.90	0.86	0.03
	F_S	0.38	0.05	0.15	0.05	0.16	0.16
	S_{GT}	0.07	0.02	0.57	0.03	0.17	0.27

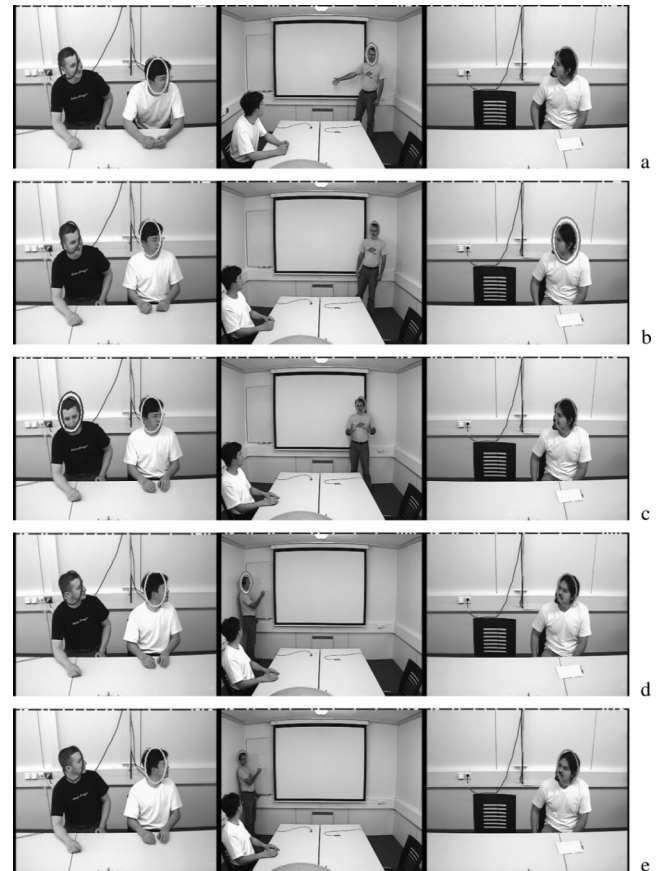


Fig. 8. Multispeaker tracking results for our approach, *meeting3*. Figure (a–e) correspond to frames 50, 490, 690, 945, and 1130, respectively.

800 with $\mathcal{I}_{800} = \emptyset$. At frame 801, the algorithm detects O1–O4 and initializes them correctly. O5 is detected at frame 825.

An objective evaluation was conducted on *meeting1* and *meeting2* to test the sole effect of automatic initialization. We consider for evaluation only those frames after which the objects have been automatically initialized, which occurs around frame 25 for *meeting1*, and around frame 1 for *meeting2*. To be able to provide a fair comparison with the results obtained for *meeting2* in Table II (i.e. keeping equivalent conditions), we set $m_t^{\max} = 4$, allowing a maximum of four objects along the



Fig. 9. Auto-initialization. (a–c) *meeting1*, frames 0, 1, and 24. (d–f) *meeting2*, frames 800, 801, and 825.

sequence. This implies that only the four first detected objects are tracked, while the fifth person is excluded from this process, as in the experiments reported in Table II. The results are shown in Table V. For *meeting1*, we observe that the performance essentially remains the same as the case of manual initialization (compare Tables I and V). For *meeting2*, we observe a minor performance degradation (compare O_{avg} in Tables II and V),

TABLE V
TRACKING RESULTS FOR *meeting1* AND *meeting2* FOR THE
MCMC-PF WITH AUTO-INITIALIZATION

<i>method</i>	<i>measure</i>	O1	O2	O3	O4	O_{avg}	$\sigma_{O_{avg}}$
<i>meeting1</i>	<i>SR</i>	1.00	1.00	1.00	1.00	1.00	0.00
	<i>TR</i>	1.00	1.00	1.00	1.00	1.00	0.00
	F_T	0.89	0.87	0.84	0.92	0.88	0.04
	F_S	0.72	0.74	0.78	0.75	0.75	0.03
<i>meeting2</i>	<i>SR</i>	1.00	0.85	1.00	1.00	0.96	0.08
	<i>TR</i>	1.00	0.98	1.00	1.00	0.99	0.01
	F_T	0.89	0.85	0.88	0.86	0.87	0.02
	F_S	0.72	0.73	0.71	0.80	0.74	0.04

which suggests that the algorithm is still effective. A more detailed evaluation of the algorithm for varying number of people would require the adaptation of our evaluation protocol to handle multiobject configuration and identification issues, which is a research topic on its own [41].

6) *Overall Discussion*: The results have shown that our framework can localize and track multiple people and their speaking status with good accuracy, tolerating visual clutter, being capable of correctly inferring some cases of simultaneous speech, and significantly outperforming a traditional PF. In particular, the interaction term model is effective to handle cases of partial occlusion, but its impact depends on the person model being accurate. Regarding visual observations, while our model seems to be adequate for the application, as stated in Section VII, it could be improved by the use of a specialized face detector algorithm (e.g., [45]), which would be specially useful for initialization purposes. For audio observations, given the use of a small microphone array, speaking activity tends to be better detected for seated speakers than for presenters; this could be seen as a tradeoff between performance and ease of sensor deployment.

IX. CONCLUSION AND FUTURE WORK

In this paper, we presented a probabilistic framework for the joint tracking of multiple people and their speaking activity in a multisensor meeting environment. Our framework integrated a novel AV observation model, a principled mechanism to represent proximity-based interactions, and an efficient sampling strategy that overcomes some of the problems faced by traditional PFs in high-dimensional state-spaces. In principle, the sensor calibration algorithm we defined puts few constraints on the sensors' location, so cameras and microphones could potentially be placed in various configurations. Several issues remain open. First, more refined interaction models could be proposed, making use of the speaking activity variable in the MRF prior, and introducing an occlusion variable in the state-space, which could explicitly define a set of switching occlusion modes. Second, although our model can reflect simultaneous speaking activity from multiple people, it is based on a limiting single-audio-source assumption. We are currently developing truly multispeaker detection techniques [26] and plan to integrate them in our framework in the future. Third, the auto-

initialization mechanism could be enhanced by using audio-based localization and/or face detection, whose integration in the MCMC-PF is conceptually direct. Finally, the evaluation on more dynamic data, including more complex cases of object birth/death, are also part of future work.

ACKNOWLEDGMENT

The authors would like to thank K. Smith (IDIAP Research Institute) for discussions, and all the participants in the meeting sequences for their time.

REFERENCES

- [1] P. Aarabi and S. Zaky, "Robust sound localization using multi-source audiovisual information fusion," *Inf. Fusion*, vol. 3, no. 2, pp. 209–223, Sep. 2001.
- [2] R. Baeza-Yates and B. Ribeiro-Neto, *Modern Information Retrieval*. New York: ACM, 1999.
- [3] M. Beal, H. Attias, and N. Jovic, "Audio-video sensor fusion with probabilistic graphical models," in *Proc. Eur. Conf. Comput. Vision (ECCV)*, May 2002, pp. 736–750.
- [4] C. Berzuini, N. Best, W. Gilks, and C. Larizza, "Dynamic conditional independence models and Markov Chain Monte Carlo methods," *J. Amer. Stat. Assoc.*, vol. 92, no. 440, pp. 1403–1412, 1997.
- [5] N. Checka, K. Wilson, M. Siracusa, and T. Darrell, "Multiple person and speaker activity tracking with a particle filter," in *Proc. IEEE Int. Conf. Acoust., Speech Signal Process. (ICASSP)*, Montreal, QC, Canada, May 2004, pp. 881–884.
- [6] Y. Chen and Y. Rui, "Real-time speaker tracking using particle filter sensor fusion," *Proc. IEEE*, vol. 92, no. 3, pp. 485–494, Mar. 2004.
- [7] R. Cutler and L. Davis, "Look who's talking: Speaker detection using video and audio correlation," in *Proc. IEEE Int. Conf. Multimedia (ICME)*, New York, Jul. 2000, pp. 1589–1592.
- [8] R. Cutler, Y. Rui, A. Gupta, J. Cadiz, I. Tashev, A. Colburn, Z. Zhang, Z. Liu, and S. Silverberg, "Distributed meetings: A meeting capture and broadcasting system," in *Proc. ACM Int. Conf. Multimedia (MM)*, Juan les Pins, Antibes, France, Dec. 2002, pp. 503–512.
- [9] J. DiBiase, H. Silverman, and M. Brandstein, "Robust localization in reverberant rooms," in *Microphone Arrays*, M. Brandstein and D. Ward, Eds. New York: Springer, 2001, ch. 8, pp. 157–180.
- [10] A. Dielmann and S. Renals, "Dynamic Bayesian networks for meeting structuring," in *Proc. IEEE Int. Conf. Acoust., Speech Signal Process. (ICASSP)*, Montreal, QC, Canada, May 2004, pp. 629–632.
- [11] A. Doucet, N. de Freitas, and N. Gordon, Eds., *Sequential Monte Carlo Methods in Practice*. New York: Springer-Verlag, 2001.
- [12] P. Fearnhead, "MCMC, sufficient statistics and particle filters," *J. Comput. Graphical Stat.*, vol. 11, pp. 848–862, 2002.
- [13] J. Fisher, T. Darrell, W. T. Freeman, and P. Viola, "Learning joint statistical models for audio-visual fusion and segregation," in *Proc. Neural Inf. Process. Syst. (NIPS)*, Denver, CO, Dec. 2000, pp. 772–778.
- [14] D. Gatica-Perez, G. Lathoud, I. McCowan, and J.-M. Odobez, "A mixed-state i-particle filter for multi-camera speaker tracking," in *Proc. IEEE Int. Conf. Comput. Vision, Workshop on Multimedia Technologies for E-Learning and Collaboration (ICCV-WOMTEC)*, Nice, France, Oct. 2003.
- [15] W. Gilks and C. Berzuini, "Following a moving target—Bayesian inference for dynamic Bayesian models," *J. R. Stat. Soc.*, ser. B, vol. 63, pp. 127–146, 2001.
- [16] S. M. Griebel and M. S. Brandstein, "Microphone array source localization using realizable delay vectors," in *Proc. IEEE Workshop Applications Signal Process. Audio Acoust. (WASPAA)*, New Paltz, NY, Oct. 2001, pp. 71–74.
- [17] J. Hershey and J. Movellan, "Audio vision: Using audio-visual synchrony to locate sounds," in *Proc. Neural Inf. Process. Syst. (NIPS)*, Denver, CO, Nov. 1999, pp. 813–819.
- [18] M. Isard and A. Blake, "CONDENSATION: Conditional density propagation for visual tracking," *Int. J. Comput. Vision*, vol. 29, no. 1, pp. 5–28, 1998.
- [19] —, "A mixed-state CONDENSATION tracker with automatic model-switching," in *Proc. IEEE Int. Conf. Comput. Vision (ICCV)*, Mumbai, India, Jan. 1998, pp. 107–112.
- [20] M. Isard and J. MacCormick, "BRAMBLE: A Bayesian multi-blob tracker," in *Proc. IEEE Int. Conf. Comput. Vision (ICCV)*, Vancouver, BC, Canada, Jul. 2001, pp. 34–41.
- [21] B. Kapralos, M. Jenkin, and E. Milios, "Audio-visual localization of multiple speakers in a video teleconferencing setting," *Int. J. Imaging Syst. Technol.*, vol. 13, pp. 95–105, 2003.
- [22] Z. Khan, T. Balch, and F. Dellaert, "An MCMC-based particle filter for tracking multiple interacting targets," in *Proc. Eur. Conf. Comput. Vision (ECCV)*, Prague, Czech Republic, May 2004, pp. 279–290.
- [23] C. Knapp and G. Carter, "The generalized correlation method for estimation of time delay," *IEEE Trans. Acoust., Speech Signal Process.*, vol. ASSP-24, no. 4, pp. 320–327, Aug. 1976.
- [24] F. Kubala, S. Colbath, D. Liu, and J. Makhoul, "Rough'n'ready: A meeting recorder and browser," *ACM Comput. Surv.*, vol. 31, no. 2es, Jun. 1999.
- [25] G. Lathoud, I. McCowan, and J.-M. Odobez, "Unsupervised location-based segmentation of multi-party speech," in *Proc. IEEE Int. Conf. Acoust., Speech, Signal Process. (ICASSP), NIST Meeting Recognition Workshop*, Montreal, May 2004.
- [26] G. Lathoud and M. Magimai-Doss, "A sector-based, frequency-domain approach to detection and localization of multiple speakers," in *Proc. IEEE Int. Conf. Acoust., Speech, Signal Process. (ICASSP)*, Philadelphia, PA, Mar. 2005, pp. 265–268.
- [27] S. Z. Li, *Markov Random Field Modeling in Computer Vision*. New York: Springer, 1995.
- [28] J. S. Liu and R. Chen, "Sequential Monte Carlo methods for dynamic systems," *J. Amer. Stat. Assoc.*, vol. 93, no. 443, pp. 1032–1044, 1998.
- [29] J. S. Liu, *Monte Carlo Strategies in Scientific Computing*. New York: Springer-Verlag, 2001.
- [30] L. Lu and H. J. Zhang, "Content analysis for audio classification and segmentation," *IEEE Trans. Speech Audio Process.*, vol. 10, no. 7, pp. 504–516, Oct. 2002.
- [31] I. McCowan, D. Gatica-Perez, S. Bengio, G. Lathoud, M. Barnard, and D. Zhang, "Automatic analysis of multimodal group actions in meetings," *IEEE Trans. Pattern Anal. Mach. Intell.*, vol. 27, no. 3, pp. 305–317, Mar. 2005.
- [32] J. E. McGrath, *Groups: Interaction and Performance*. Englewood Cliffs, NJ: Prentice-Hall, 1984.
- [33] N. Morgan, D. Baron, J. Edwards, D. Ellis, D. Gelbart, A. Janin, T. Pfau, E. Shriberg, and A. Stolcke, "The meeting project at ICSI," in *Proc. Human Language Technology Conf. (HLT)*, San Diego, CA, Mar. 2001, pp. 1–7.
- [34] D. Moore, The IDIAP smart meeting room IDIAP Res. Inst., Martigny, Switzerland, IDIAP-COM 07, 2002.
- [35] V. Pavlovic, A. Garg, and J. Rehg, "Multimodal speaker detection using error feedback dynamic bayesian networks," in *Proc. IEEE Conf. Comput. Vision Pattern Recognition (CVPR)*, Hilton Head Island, SC, 2000, pp. 34–41.
- [36] P. Perez, C. Hue, J. Vermaak, and M. Gangnet, "Color-based probabilistic tracking," in *Proc. Eur. Conf. Comput. Vision (ECCV)*, Copenhagen, Denmark, May 2002, pp. 661–675.
- [37] G. S. Pingali, G. Tunali, and I. Carlbom, "Audio-visual tracking for natural interactivity," in *Proc. ACM Int. Conf. Multimedia (MM)*, Orlando, FL, Oct. 1999, pp. 373–382.
- [38] I. Potamitis, H. Chen, and G. Tremouliis, "Tracking of multiple moving speakers with multiple microphone arrays," *IEEE Trans. Speech Audio Process.*, vol. 12, no. 5, pp. 520–529, Sep. 2004.
- [39] E. Shriberg, A. Stolcke, and D. Baron, "Observations on overlap: Findings and implications for automatic processing of multi-party conversation," in *Proc. Eur. Conf. Speech Comm. Technol. (Eurospeech)*, Aalborg, Denmark, Sep. 2001, pp. 1359–1362.
- [40] M. Siracusa, L.-P. Morency, K. Wilson, J. Fisher, and T. Darrell, "A multi-modal approach for determining speaker location and focus," in *Proc. Int. Conf. Multimodal Interfaces (ICMI)*, Vancouver, BC, Canada, 2003, pp. 77–80.
- [41] K. Smith, D. Gatica-Perez, J.-M. Odobez, and S. Ba, "Evaluating multi-object tracking," in *Proc. IEEE CVPR Workshop on Empirical Evaluation Methods on Computer Vision (CVPR-EEMCV)*, San Diego, CA, Jun. 2005, pp. 36–43.
- [42] R. Stiefelwagen, J. Yang, and A. Waibel, "Modeling focus of attention for meeting indexing based on multiple cues," *IEEE Trans. Neural Netw.*, vol. 13, no. 4, pp. 928–938, Jul. 2002.

- [43] D. Sturim, M. Brandstein, and H. Silverman, "Tracking multiple talkers using microphone array measurements," in *Proc. IEEE Int. Conf. Acoust., Speech, Signal Process. (ICASSP)*, Munich, Germany, Apr. 1997, pp. 371–374.
- [44] J. Vermaak, M. Gagnet, A. Blake, and P. Perez, "Sequential Monte Carlo fusion of sound and vision for speaker tracking," in *Proc. IEEE Int. Conf. Comput. Vision (ICCV)*, Vancouver, BC, Canada, Jul. 2001, pp. 741–746.
- [45] P. Viola and M. Jones, "Rapid object detection using a boosted cascade of simple features," in *Proc. IEEE Conf. Comput. Vision Pattern Recognition (CVPR)*, Kauai, HI, Dec. 2001, pp. 511–518.
- [46] B. Vo, S. Singh, and W. K. Ma, "Tracking multiple speakers using random sets," in *Proc. IEEE Int. Conf. Acoust., Speech, Signal Process. (ICASSP)*, Montreal, QC, Canada, May 2004, pp. 357–360.
- [47] A. Waibel, M. Bett, F. Metzger, K. Ries, T. Schaaf, T. Schultz, H. Soltan, H. Yu, and K. Zechner, "Advances in automatic meeting record creation and access," in *Proc. IEEE Int. Conf. Acoust., Speech, Signal Process. (ICASSP)*, Salt Lake City, UT, May 2001, pp. 597–600.
- [48] D. B. Ward, E. A. Lehmann, and R. C. Williamson, "Particle filtering algorithms for acoustic source localization," *IEEE Trans. Speech Audio Process.*, vol. 11, no. 6, pp. 826–836, Nov. 2003.
- [49] B. Wrede and E. Striberg, "The relationship between dialogue acts and hot spots in meetings," in *Proc. IEEE Automatic Speech Recognition and Understanding Workshop (ASRU)*, Virgin Islands, Dec. 2003, pp. 180–185.
- [50] D. Zotkin, R. Duraiswami, and L. Davis, "Multimodal 3-D tracking and event detection via the particle filter," in *IEEE ICCV Workshop on Detection and Recognition of Events in Video (ICCV-EVENT)*, Vancouver, BC, Canada, Jul. 2001, pp. 20–27.



Daniel Gatica-Perez (S'01–M'02) received the B.S. degree in electronic engineering from the University of Puebla, Puebla, Mexico, in 1993, the M.S. degree in electrical engineering from the National University of Mexico, Mexico City, in 1996, and the Ph.D. degree in electrical engineering from the University of Washington, Seattle, in 2001.

He joined the IDIAP Research Institute, Martigny, Switzerland, in January 2002, where he is now a Senior Researcher. His interests include multimedia signal processing and information retrieval, computer vision, and statistical machine learning applied to these domains.



Guillaume Lathoud received the M.Sc. degree in computer science and telecommunications from the Institut National des Télécommunications (INT), Evry, France, in 1999.

He then spent more than two years as a member of the Digital Television Team, National Institute of Standards and Technology (NIST), Gaithersburg, MD, participating to terrestrial DTV standardization and implementation efforts. He joined the IDIAP Research Institute, Martigny, Switzerland, in 2002 as a Ph.D. student. His interests include microphone

array processing, audio source localization, speaker tracking, multimodal processing, and noise-robust speech recognition.



Jean-Marc Odobez (M'03) was born in France in 1968. He graduated from the Ecole Nationale Supérieure des Télécommunications de Bretagne (ENSTBr) in 1990, and received the Ph.D. degree in signal processing and telecommunications from the Université de Rennes, Rennes, France, in 1994 with a dissertation on dynamic scene analysis.

He spent one year as a Postdoctoral Fellow at the GRASP Laboratory, University of Pennsylvania, Philadelphia, working on visually guided navigation problems. From 1996 until 2001, he was an

Associate Professor at the Université du Maine, Le Mans, France. In 2001, he joined the IDIAP Research Institute, Martigny, Switzerland, as a Senior Researcher, where he is working on the development of statistical methods and machine learning algorithms for multimedia signal analysis and computer vision problems.



Iain McCowan (M'97) received the B.E. and B.InfoTech. degrees from the Queensland University of Technology (QUT), Brisbane, Australia, in 1996. In 2001, he completed his Ph.D. degree with the Research Concentration in Speech, Audio and Video Technology at QUT, including a period of research at France Telecom, Lannion.

He joined the IDIAP Research Institute, Martigny, Switzerland, in April 2001, as a Research Scientist, progressing to the post of Senior Researcher in 2003.

While at IDIAP, he worked on a number of applied research projects in the areas of automatic speech recognition and multimedia content analysis, in collaboration with a variety of academic and industrial partner sites. From January 2004 to 2005, he was Scientific Coordinator of the EU Augmented Multi-Party Interaction (AMI) project, jointly managed by IDIAP and the University of Edinburgh. He joined the CSIRO eHealth Research Centre, Brisbane, in May 2005, as Project Leader in Multimedia Content Analysis.